Original

Bakardzhiev, P.; Rangelov, S.; Trzebicka, B.; Momekova, D.; Lalev, G.; Haramus, V.M.:

Nanostructures by self-assembly of polyglycidol-derivatized lipids

In: RSC Advances (2014) Royal Society of Chemistry

DOI: 10.1039/c4ra03102d

RSC Advances

PAPER

View Article Online
View Journal | View Issue

Cite this: *RSC Adv.*, 2014, **4**, 37208

Nanostructures by self-assembly of polyglycidol-derivatized lipids†

Pavel Bakardzhiev,*[a] Stanislav Rangelov,[a] Barbara Trzebicka,[b] Denitsa Momekova,[c] Georgi Lalev[ad] and Vasil M. Garamus[e]

Received 7th April 2014
Accepted 13th August 2014

DOI: 10.1039/c4ra03102d

www.rsc.org/advances

In this work we report on the self-assembly of five non-phospholipid polyglycidol conjugates in aqueous solution. The polymers are composed of a linear polyglycidol chain (degrees of polymerization, DP, are in the 8–110 range) linked to a strongly hydrophobic lipid-mimetic residue. Their behavior in dilute aqueous solution is investigated by a combination of experimental techniques – UV-vis spectroscopy, static and dynamic light scattering, fluorescence measurements, conventional and cryogenic transmission electron microscopy, and small angle X-ray scattering. The polymers spontaneously self-associate above a certain critical concentration, which depends on polyglycidol DP and temperature. According to the thermodynamic data, the self-assembly is an enthalpically disfavored endothermic process, driven by positive entropy contribution. The polymers with polyglycidol DP of 23 and above form small core–corona micelles. The latter are parameterized and the experimental values are compared to those of micelles of the commercially available poly(ethylene glycol)-derivatized lipids and other related non-phospholipid poly(ethylene glycol) conjugates. The polymer of the lowest polyglycidol DP form lamellar structures of co-existing morphology – spherical vesicles and highly anisotropic, elongated bilayer flakes.

Introduction

Poly(ethylene glycol) (PEG) derivatized phospholipids have found an important application to provide steric stabilization and stealth properties of lipid vesicles (liposomes) resulting in prolongation of their blood circulation time.[1–8] These products (hereinafter PEG–lipids) are nowadays commercially available in a variety of molar masses of the PEG chain (from 350 to 5000) and diversity of lipid anchors – 1,2-distearoylphosphatidylethanolamine, 1,2-dipalmitoylphosphatidylethanolamine, 1-palmitoyl-2-oleylphosphatidylethanolamine, *etc.* Being composed of a strongly hydrophobic phospholipid residue and a hydrophilic PEG chain, the PEG–lipids exhibit amphiphilic properties: in dilute aqueous solution and above a certain critical concentration, they form small spherical micelles,[9–12] which have been carefully investigated and parametrized.[13] Recent atomistic molecular dynamic simulations have revealed that the micelles of PEG-conjugated 1,2-distearoylphosphatidylethanolamine in water consist of a hydrophobic core with a relatively sharp boundary, an ionic interface, and a semipolar PEG corona.[14] There are also studies reporting formation of lamellar phases at low to moderate temperatures that co-exist with the micelles.[1,13] The lamellar phase is dominating for PEG–lipids with low molar mass PEG.[9]

Enhancement of the longevity of liposomes is usually achieved by anchoring the lipid residue of PEG–lipids in the bilayer membrane, whereas the PEG chains create a repulsive barrier around the liposomes. However, as a result of the intercalation of the PEG–lipids, a net negative charge is introduced at the bilayer membrane surface, which has been reported to play a key role in complement activation and anaphylotoxin production[15] in addition to substantial alteration of the properties and performance of the liposomes.[16,17] Furthermore, the negative charge of the phosphoryl moiety of phospholipids has been frequently related to many hypersensitivity reactions observed with the usage of intravenous liposome products.[18,19] The biological reactivity as well as relative instability and the costs associated with extraction and synthesis of phospholipids[20,21] justify the interest for development of lipid bilayer vesicle delivery systems using lipid amphiphiles other than phospholipids.[22] In that aspect, higher biological acceptability of

[a]*Institute of Polymers, Bulgarian Academy of Sciences, Acad. G. Bonchev Str. 103-A, 1113 Sofia, Bulgaria. E-mail: p.borisov@polymer.bas.bg*

[b]*Centre of Polymer and Carbon Materials, Polish Academy of Sciences, M. Curie-Sklodowskiej 34, 41-819 Zabrze, Poland*

[c]*Department of Pharmaceutical Technology and Biopharmaceutics, Faculty of Pharmacy, Medical University – Sofia, Dunav Str. 2, 1000 Sofia, Bulgaria*

[d]*School of Chemistry, Cardiff University, Cardiff, CF10 3AT, UK*

[e]*Helmholtz-Zentrum Geesthacht, Max-Planck Str 1., 21502 Geesthacht, Germany*

† Electronic supplementary information (ESI) available: Detailed description of the synthetic procedure including a reaction scheme as well as GPC and ^{1}H NMR characterization data. Additional experimental data from light scattering include relaxation time distributions as well as plots of relaxation rate as a function of $\sin^2(\theta/2)$, concentration dependence of diffusion coefficients and reduced scattered light intensity *vs.* concentration. See DOI: 10.1039/c4ra03102d

synthetic polymer-derivatized lipids devoid of phosphoryl moiety can be hypothesized. Earlier efforts to prepare non-phospholipid PEG conjugates have been made by Rangelov *et al.*[23] These completely non-ionic conjugates are composed of a PEG chain of degrees of polymerization (DP) in the 30–92 range attached to a lipid-mimetic residue, consisting of two C_{12} fully saturated hydrocarbon chains covalently linked to a glycerol skeleton *via* ether linkages. Complete physicochemical characterization of the self-assembled structures formed in water has been carried out as well.[23] In another paper, Nag *et al.*[24] have reported synthesis and characterization of novel PEG-conjugated hexadecyl-carbamoylmethyl hexadecanoate as a PEG–phospholipid substitute for enhancing circulation persistence of liposomes.

Obviously, PEG is the hydrophilic polymer of choice to be conjugated to either a phospholipid or non-phospholipid residue. The information about usage of other polymers is scarce. To the best of authors' knowledge poly(*N*-isopropylacrylamide) and poly(2-alkyl-2-oxazoline) have occasionally been used as PEG substitutes.[25–29] Linear polyglycidol is structurally similar to PEG. In contrast to the latter, it bears a hydroxymethylene group in each repeating monomer unit (see Scheme 1 below for the structural formula of polyglycidol). Polyglycidol is non-toxic and biocompatible[30] and, hence, constitutes a potential platform for a variety of medical, pharmaceutical, biochemical, and biotechnological applications. A recent series of articles have focused on the synthesis and aqueous solution properties of novel polyglycidol–poly(propylene oxide)–polyglycidol (LGP) triblock copolymers,[31–37] which can be considered analogues of the commercially available Pluronic, poly(ethylene oxide)–poly(propylene oxide)–poly(ethylene oxide), copolymers. It is remarkable that small alterations in the chemical structure of the hydrophilic blocks, *i.e.*, introduction of a hydroxymethylene group, are manifested in significant differences in the aqueous solution properties of the two groups of copolymers. The influence of the molar mass of the central block of poly(propylene oxide) has been assessed as well.[37] In the attempts to diversify not only the lipidic residue but also the polymer chain, we synthesised a series of novel non-phospholipid polyglycidol conjugates. Their structural formula and molecular characteristics are presented in Scheme 1 and Table 1, respectively. We set out to investigate their self-assembly in aqueous solution and to characterize the aggregates that are formed using a combination of experimental techniques. The results obtained are compared with those of related phospholipid and non-phospholipid conjugates based on PEG. In forthcoming articles we will present other polyglycidol-lipids devoid of phosphoryl moiety as substitutes of the conventional PEG–lipids and their potential to form Stealth liposomes.

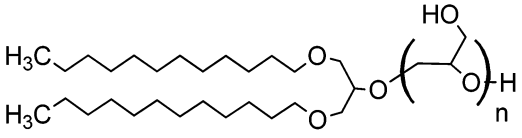

Scheme 1 Chemical structure of the investigated polyglycidol-derivatized lipids, DDP-$(G)_n$. DDP: 1,3-didodecyl/tetradecyloxy-propane-2-ol; G: glycidol monomeric unit.

Table 1 Composition and nominal molar masses of the investigated polyglycidol-derivatized lipids

Composition	Nominal molar mass ($g\ mol^{-1}$)
DDP-$(G)_8$	1020
DDP-$(G)_{23}$	2130
DDP-$(G)_{30}$	2650
DDP-$(G)_{54}$	4420
DDP-$(G)_{110}$	8570

Experimental section

Materials

All solvents (methanol, dichloromethane) as well as ethyl vinyl ether (99%, Aldrich) were purified by distillation. Glycidol (96% Aldrich) was distilled under vacuum. $AlCl_3 \cdot 6H_2O$ (99%, Aldrich), KOH (Merck), 1-dodecanol (Aldrich), 1,6-diphenyl-1,3,5-hexatriene (Aldrich), 5(6)-carboxyfluorescein (Aldrich), and dodecyl/tetradecyl glycidyl ether (Aldrich) were used without purification. The starting alcohol, 1,3-didodecyl/tetradecyloxy-propane-2-ol (DDP), was prepared according to a procedure described elsewhere.[38] Ethoxyethyl glycidyl ether (EEGE) was obtained by a reaction of glycidol and ethyl vinyl ether as described elsewhere.[39] The synthesis and characterization of the DDP-$(G)_n$ polymers are presented in details in the ESI.†

Analyses and methods

Determination of the critical micellization concentration (CMC). Aqueous solutions (2.0 mL) of a given polymer in the concentration range from 0.001 to 5 wt % were prepared at room temperature. 20 μL of a 0.4 mM solution of 1,6-diphenyl-1,3,5-hexatriene (DPH) in methanol was added to each of the copolymer solutions. The solutions were incubated in the dark for 16 h at room temperature. The absorbance in the wavelength interval $\lambda = 300$–500 nm was followed at temperatures ranging from 20 to 60 °C on a Beckman Coulter DU 800 UV-vis spectrometer. The main absorption peak, characteristic for DPH solubilized in a hydrophobic environment, was at 356 nm.

Dynamic light scattering (DLS). DLS measurements were performed on a Brookhaven BI-200 goniometer with vertically polarized incident light at a wavelength $\lambda = 632.8$ nm supplied by a He–Ne laser operating at 35 mW and equipped with a Brookhaven BI-9000 AT digital autocorrelator. The scattered light was measured for dilute aqueous solutions of the investigated polymers in the concentration range 0.161–12.24 mg mL^{-1}. Measurements were made at angles θ in the range of 50–130°. The autocorrelation functions were analyzed using the constrained regularized algorithm CONTIN[40] to obtain the distributions of the relaxation rates (Γ). The latter provided distributions of the apparent diffusion coefficient ($D = \Gamma/q^2$)

where q is the magnitude of the scattering vector given by $q = (4\pi n/\lambda)\sin(\theta/2)$, n is the refractive index of the medium. The mean hydrodynamic radius was obtained by the Stokes–Einstein eqn (1):

$$R_h = kT/(6\pi\eta D_0) \quad (1)$$

where k is the Boltzman constant, η is the solvent viscosity at temperature T in Kelvin and D_0 is the diffusion coefficient at infinite dilution.

Static light scattering (SLS). The SLS measurements were carried out in the interval of angles from 40 to 140° at 25 °C and for some of the samples at 37 °C using the same light scattering set. The SLS data were analyzed using the Berry plot software provided by Brookhaven Instruments. Information on the weight-average molar mass, M_w, the radius of gyration, R_g, and the second virial coefficient, A_2, was obtained from the dependence of the quantity $(Kc/R_\theta)^{1/2}$ on the concentration (c) and scattering angle (θ). Here, K is the optical constant and R_θ is the Rayleigh ratio at θ. For small particles (isotropic scatterer) when no intramolecular interference is present, and the intensity of scattered light is angularly independent, both the weight-average molar masses, and the second virial coefficients were determined from the dependence of $Kc/R_{\theta=90}$ *vs.* concentration. In the SLS calculations, the refractive index increment (dn/dc) values measured in water in separate experiments were used.

Small-angle X-ray scattering (SAXS). The SAXS experiments were conducted on a Nanostar (Bruker AXS GmbH, Karlsruhe, Germany) laboratory small-angle X-ray diffractometer with the following characteristic parameters: microfocus X-ray source IμS, the used Cu Kα wavelength of 1.54 Å, detector VANTEC-2000 (14 × 14 cm in size, resolution of 2048 × 2048 pixels), and the sample-detector distance of 103 cm. The samples were placed into glass capillary vessels with a diameter of 2 mm. The primary processing of data with taking into account the scattering from the solvent and capillary, detector efficiency, and background signal, as well as the recalculation to the absolute cross sections, was performed with the SuperSAXS (Jan Pedersen&Cristiano Oliveira) code.

Leakage assay. Fluorescent measurements, with the fluorescent probe 5(6)-carboxyfluorescein (CF), were carried out on a Hitachi F-7000 fluorescence spectrophotometer. The fluorescent intensity, I, was measured as a function of time at 520 nm with excitation at 490 nm. The measurements were performed at 37 °C. The samples of DDP-$(G)_8$ of concentration 5 mg mL^{-1} were prepared in an aqueous medium containing 100 mM CF and at pH 7.4. The unentrapped dye was removed by gel filtration using a Sephadex G-50 column. The leakage was followed on the time scale of 6–7 hours. Then, the maximal intensity, I_{max}, was obtained after lysis of the vesicles with a surfactant added to the dispersion from a stock solution.

Transmission electron microscopy (TEM) and cryogenic transmission electron microscopy (cryo-TEM). To provide detailed morphological and compositional information about the studied samples at micro and nano-scale, high-resolution transmission electron microscope (HR-TEM) system JEOL 2100 (LaB6) was employed. The state-of-the-art instrument is equipped with high-resolution Gatan digital camera (2k × 2k) providing resolution of 0.2 Å which makes possible detailed observation of the objects, obtaining diffraction pattern and accurate measurements of the lattice d-spacing with the help of Digital Micrograph software. For the purpose of the cryo analysis, the samples were pre-frozen in liquid nitrogen by plunge freezing and transferred on high-tilt Gatan cryo transfer tomography holder (Model 914) using Gatan cryo station. The holder is specifically designed for analysis of frozen samples for biological and polymer application. To maintain the temperature of −175 °C, the holder is equipped with cryo dewar for liquid nitrogen having zeolite cryopump inside. During the experiments, the sample temperature was constantly monitored by Gatan SmartSet cold stage controller (Model 900). For HR-TEM analysis, after preparing a water suspension from the samples, a drop of about 8 μL was put on the TEM grid and dried. For cryo-TEM analysis, the grid was blotted with filter paper to remove the excess of suspension and immediately plunged in liquid ethane and then dipped in liquid nitrogen. The pre-frozen sample was transferred to Gatan cryo station where the TEM grid was mounted on Gatan cryo holder without exposing the sample to air.

Results and discussion

Aqueous solution properties, in particular, determination of the critical micellization concentrations and thermodynamic parameters of self-assembly as well as the static and dynamic light scattering parameters of the resulting particles and their visualization by electron microscopy are presented in order to get some insight into the nature and behavior of the original polymers.

Determination of the critical micellization concentrations (CMCs)

For determination of the CMCs at different temperatures the properties of 1,6-diphenyl-1,3,5-hexatriene (DPH) were exploited. DPH is a hydrophobic dye, which is sensitive to changes in the microenvironment: its absorbance is minimal in water, whereas in hydrophobic environments substantially increases showing a characteristic maximum at 356 nm. DPH has been employed for determination of CMC of conventional and polymeric surfactants,[41–45] including copolymers based on polyglycidol.[31,35,37] Fig. 1a shows UV-vis absorption spectra of DPH in the presence of increasing amounts of DDP-$(G)_{30}$ taken at 20 °C. The appearance of maxima at 356 nm indicated the presence of hydrophobic domains. The CMC values were determined from the break of the intensity *vs.* concentration curves as shown in Fig. 1b. The CMC values of all polymers were determined at four temperatures – 20, 37, 50 and 60 °C. The variations with temperature and DP of polyglycidol are presented in Fig. 2. As Fig. 2a clearly shows, the CMCs of the polymers of lower DP are only slightly affected by temperature. The effect of temperature became more visible with increasing DP and was most strongly pronounced for the polymer of the highest DP of polyglycidol – DDP-$(G)_{110}$. These results are somewhat unexpected, since the

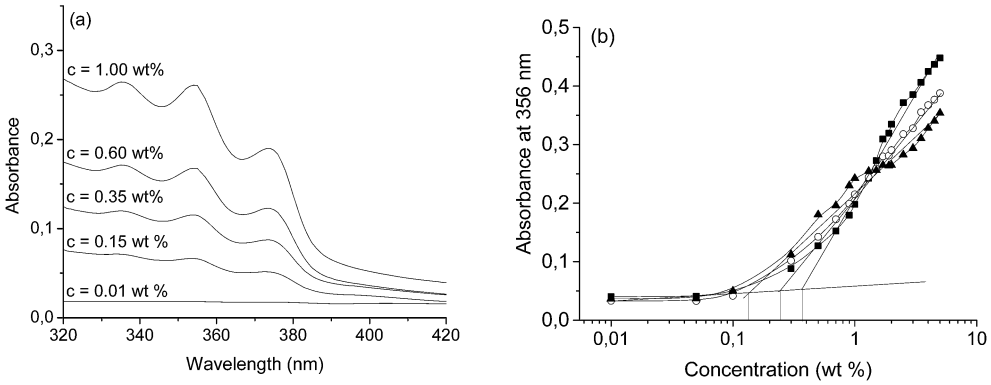

Fig. 1 (a) Effect of DDP-$(G)_{30}$ concentration on UV-vis absorption spectra of 1,6-diphenyl-1,3,5-hexatriene (DPH) taken at 20 °C. (b) Absorbance at 356 nm *vs.* DDP-$(G)_{54}$ concentration at 20 (squares), 37 (circles), and 60 (triangles) °C.

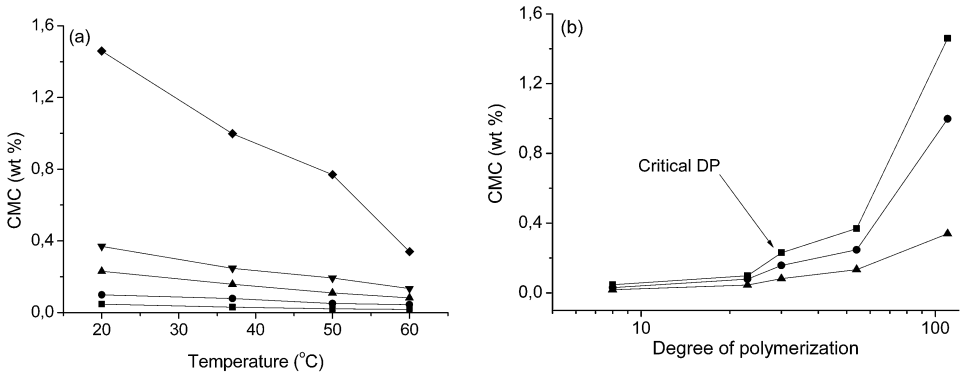

Fig. 2 Critical micellization concentrations (CMCs) as a function of (a) temperature and (b) degree of polymerization of polyglycidol chain. Symbols in (a): DDP-$(G)_8$ (squares), DDP-$(G)_{23}$ (circles), DDP-$(G)_{30}$ (triangles), DDP-$(G)_{54}$ (inverted triangles) and DDP-(G)110 (diamonds); symbols in (b): 20 °C (squares), 37 °C (circles) and 60 °C (triangles).

lipid-mimetic anchor is truly hydrophobic, that is, its interactions with water are unfavorable at all temperatures, whereas, as shown previously,[31–37] the solubility of polyglycidol increases with increasing temperature. In other words, one would expect an increase of CMCs with increasing temperature. Instead, just the opposite, being most pronounced for DDP-$(G)_{110}$, was observed for the present polymers. This finding can be rationalized recalling that at lower temperatures polyglycidol exhibits behavior that is closer to that for polymer coils in marginal solvents.[46] At such conditions DDP and polyglycidol chains are not fully segregated and we can speculate that the polyglycidol chain partially covers the lipid mimetic anchor thus effectively decreasing the portion of DDP that is exposed to water; the longer the chain, the smaller the portion (Scheme 2). At elevated temperatures the solubility of polyglycidol increases; it goes preferentially in the aqueous phase thus exposing the whole hydrophobic anchor to water (Scheme 2), which is expected to facilitate the self-assembly and to decrease the CMCs. The effect of temperature on CMC is larger for the polymers of higher DPs of polyglycidol chain – most pronounced for DDP-$(G)_{110}$ – because of the more substantial rearrangement of the macromolecules upon increasing temperature (Scheme 2).

The CMC data were re-plotted in Fig. 2b as a function of DP of the polyglycidol chain. There was a critical DP at which the curves departed from the lower region of CMCs. It is noteworthy that this degree of polymerization is 30, that is, very close to the critical DPs of 26–27 observed for polyglycidol-poly(propylene oxide)-polyglycidol copolymers studied earlier[31,35] at which the properties of the polyglycidol moieties become more significant and, accordingly, the copolymers become more hydrophilic and the self-assembly is hindered.

Thermodynamics of self-association

The thermodynamic parameters of self-assembly can be extracted from the temperature dependence of the CMC[47] using eqn (2) and (3):

$$\Delta G^\circ = RT \ln(X_{CMC}) \quad (2)$$

$$\Delta G^\circ = \Delta H^\circ - T\Delta S^\circ \quad (3)$$

where ΔG° is the free energy of association, R is the gas law constant, T is the temperature in K, X_{CMC} is the CMC in mole fractions at temperature T, and ΔH° and ΔS° are the standard enthalpy and entropy of association, respectively. ΔG° values for

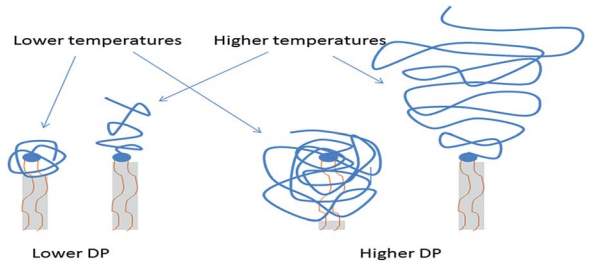

Scheme 2 Schematic presentation of rearrangements of the macromolecules of DDP-$(G)_n$ of different degrees of polymerization of the polyglycidol chain at lower and higher temperatures. The portion of lipid-mimetic anchor that is exposed to water is marked with grey.

all polymers studied are plotted as a function of temperature in Fig. 3. The negative values indicate that the process of self-association is spontaneous and more favorable (more negative values) at elevated temperatures. ΔH° and ΔS° were determined according to eqn (3) and the values are collected in Table 2.

The positive values of ΔH° indicate that the aggregation is an enthalpically disfavored endothermic process, for which the driving force is the positive entropy contribution. In contrast to the related LGP copolymers,[31,35,37] no clear trend for variations of ΔH° and ΔS° with the DP of polyglycidol was observed; instead, the values scattered in the ranges of 16–30 kJ mol^{-1} and 0.15–0.19 kJ mol^{-1} K^{-1} for ΔH° and ΔS°, respectively. The unsystematic variations of ΔH° and ΔS° most probably reflect inproportional exposure of the hydrophobic anchor to water at different temperatures and DPs of the polyglycidol chain.

Dimensions, molar masses, and aggregation number

Light scattering experiments were performed in concentration ranges above the CMC at 25 and 37 °C to determine dimensions, molar masses, aggregation numbers as well as other static and dynamic light scattering parameters. No special protocols were applied to prepare the solutions. The polymers spontaneously self-associated upon the contact with water. The solutions were left overnight at room temperature and filtered before measurements through 450 nm pore size filters to remove the dust and large metastable aggregates, which are responsible for the presence of low-amplitude slow modes[1,9,10,13,23,48–50] (see ESI†).

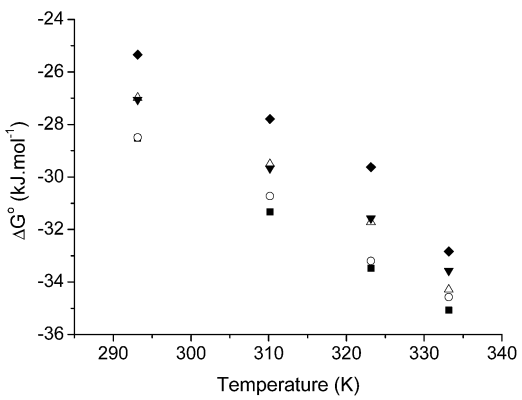

Fig. 3 Free energy of association, ΔG°, as a function of temperature for DDP-$(G)_8$ (squares), DDP-$(G)_{23}$ (circles), DDP-$(G)_{30}$ (triangles), DDP-$(G)_{54}$ (inverted triangles) and DDP-$(G)_{110}$ (diamonds).

Table 2 Standard enthalpy (ΔH°) and entropy (ΔS°) of association of the investigated DDP-polyglycidol polymers in aqueous solution

Polymer	ΔH° (kJ mol^{-1})	ΔS° (kJ mol^{-1} K^{-1})
DDP-$(G)_8$	19.52 ± 0.25	0.16 ± 0.001
DDP-$(G)_{23}$	16.44 ± 3.12	0.15 ± 0.01
DDP-$(G)_{30}$	27.23 ± 5.15	0.18 ± 0.02
DDP-$(G)_{54}$	20.81 ± 1.39	0.16 ± 0.004
DDP-$(G)_{110}$	30.41 ± 6.58	0.19 ± 0.02

Polymers DDP-$(G)_{23}$, DDP-$(G)_{30}$, DDP-$(G)_{54}$, and DDP-$(G)_{110}$ exhibited monomodal relaxation time distributions from DLS implying formation of one population of nearly uniform particles. A representative relaxation time distribution of DDP-$(G)_{23}$ is shown in Fig. 4a. The relaxation rates showed a linear dependence on $\sin^2(\theta/2)$ passing through the origin (Fig. 4b), satisfying the equation $\Gamma = Dq^2$, which confirmed the diffusive character of the particles. The diffusion coefficients were determined from the slopes of the linear fit to the data, then plotted against concentration and extrapolated to zero aggregate concentration (Fig. 4c). The values of D_0 thus obtained were used to calculate the hydrodynamic radii using the equation of Stokes–Einstein. D_0 and R_h values are collected in Table 3. Similarly to the commercially available PEG–lipids[13] as well as DDP–PEG polymers reported earlier,[23] the particles that the present polymers form are in the low nm scale. As they are small relative to the wavelength, no angular dependence of the scattered light intensity was found. Therefore, the weight-average molar masses, M_w, and the second virial coefficients, A_2, were determined from the dependence of the reduced scattered light intensity at $\theta = 90^\circ$, Kc/R_{90}, *versus* the polymer concentration. A representative plot is shown in Fig. 5 and the derived static light scattering parameters are summarized in Table 3. More relaxation time distributions and plots for determination of the static and dynamic light scattering parameters are available in ESI.†

Previous studies have indicated that polymers composed of a small lipophilic residue and comparably long polymer chains such as PEG–lipids[13,49,51] and DDP–PEG[23] form small spherical micelles. The dimensions of the aggregates that DDP-$(G)_{23}$, DDP-$(G)_{30}$, DDP-$(G)_{54}$, and DDP-$(G)_{110}$ form are in the low nm scale and are fairly consistent with the hydrodynamic dimensions of the former polymers:[13,23,49,51] R_h varied from 51 to 79 Å at 25 °C and was found to increase with increasing DP of the polyglycidol chain (Table 3). The second virial coefficients are invariably positive, indicating favorable micelle/solvent interactions. Compared to A_2 values of related systems,[13,23,49,51] they are slightly smaller in magnitude, which is in line with the lower water solubility of polyglycidol at lower temperatures (see above). The noticeable increase of A_2 at 37 °C is also consistent with this finding and implies more favorable micelle/solvent

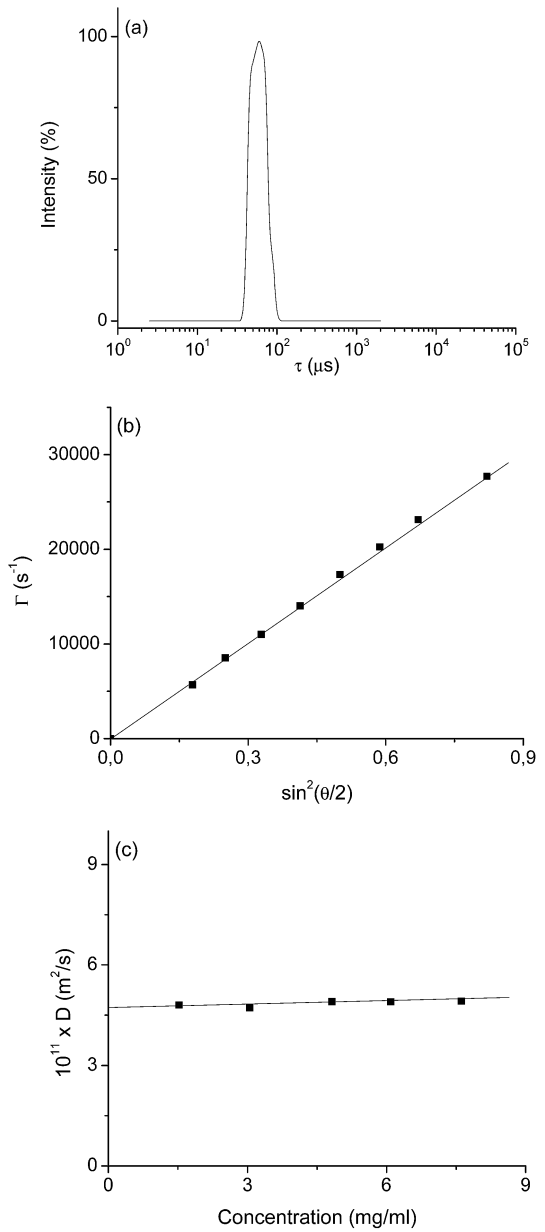

Fig. 4 (a) Representative relaxation time distribution measured at an angle of 90° for aqueous solution of DDP-$(G)_{23}$ at $c = 7.617$ mg mL^{-1} and 25 °C. (b) Relaxation rate (Γ) as a function of $\sin^2(\theta/2)$ for DDP-$(G)_{23}$ in water at $c = 7.617$ mg mL^{-1} and 25 °C. (c) Concentration dependence of the diffusion coefficients for DDP-$(G)_{23}$. The lines through the data points in (b) and (c) represent the linear fits to the data.

Table 3 Characterization data and static and dynamic light scattering parameters of nonionic DDP-polyglycidol aggregates in water at 25 °C

Polymer	$10^{11}D$ (m^2 s^{-1})	R_h (Å)	10^5A_2 (mol mL g^{-2})	$10^{-5}M_w$ (g mol^{-1})	N_{agg}[a]
DDP-$(G)_{23}$	4.73	52	6.40	1.82	91
DDP-$(G)_{30}$	4.84	51	8.66	1.58	42
	6.51[b]	50[b]	11.47[b]	1.67[b]	45[b]
DDP-$(G)_{54}$	3.75	65	7.70	1.30	31
DDP-$(G)_{110}$	3.09	79	8.95	2.54	22
	3.82[b]	86[b]	10.88[b]	2.39[b]	20[b]

[a] Aggregation number. [b] Measurements done at 37 °C.

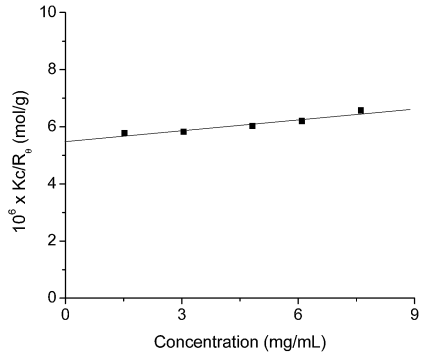

Fig. 5 Reduced scattered light intensity measured at an angle of 90°, Kc/R_{90}, as a function of concentration of DDP-$(G)_{23}$ at 25 °C.

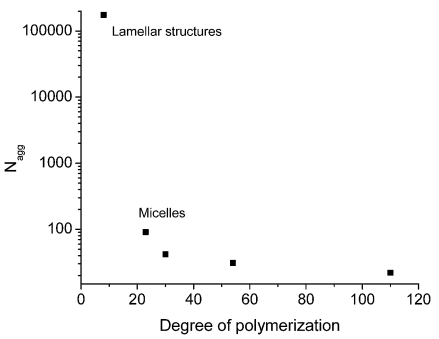

Fig. 6 Aggregation numbers (N_{agg}) determined at 25 °C of DDP-$(G)_n$ aggregates as a function of degree of polymerization of polyglycidol.

interactions at such conditions. M_w values are of the same order of magnitude as those of related systems.[13,23,49,51] The aggregation numbers (N_{agg}) were estimated using the nominal molar masses of the polymers. They are in the range of 22–91 macromolecules per particle for these four polymers and were found to increase exponentially with decreasing DP (see Fig. 6 and the section for DDP-$(G)_8$). The effect of temperature on N_{agg} and R_h is slight and somewhat ambiguous and may reflect the influence of oppositely acting factors – increasing solubility of polyglycidol moieties and exposing different portions of the lipid-mimetic anchor to water (see above).

Particle structure

The static and dynamic parameters can be used to determine geometric parameters of the self-assembled structures such as the thickness of the polyglycidol corona as well as the area of the polymer chain on the surface of the aggregates and on the core–corona interface (Scheme 3). To determine the corona thickness the radius of the core, R_c, must be known. R_c can be estimated using the experimental data for N_{agg} and the value for the lipid-

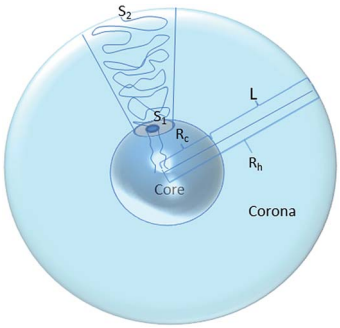

Scheme 3 Schematic presentation of a spherical micelle formed by DDP-$(G)_n$ polymers (n = 23–110) and various parameters, characterizing the micelles: hydrodynamic radius (R_h), core radius (R_c), corona thickness (L), areas occupied by polyglycidol chains on the core/corona interface (S_1) and on the outermost interface of the micelles (S_2).

mimetic anchor volume. The latter was calculated by summing up the individual group volumes as follows[52] (data in Å^3): 53.9 (CH_3), 28.4 (CH_2), 68.8 (glycerol). The overall volume of the DDP residue is 801.4 Å^3. By multiplying the DDP residue volume with N_{agg}, we got the volume of the core, V_c, from which, assuming a spherical shape of the micelles, R_c was calculated. Using the experimental data for R_h and the estimated R_c, the hydrodynamic corona thickness, L, is given by eqn (4) and graphically presented in Scheme 3:

$$L = R_h - R_c \quad (4)$$

The values of V_c, R_c, and L thus determined are collected in Table 4. Data for related polymers based on PEG are also given in Table 4 in order to compare the aggregate parameters. Generally, the micelles that DDP-$(G)_n$ polymers form are characterized with smaller core radii and larger corona thicknesses than those of the polymers based on PEG. This is strongly reflected in the values of the L/R_c ratio (last column of Table 4), which are invariably the largest for the micelles of DDP-$(G)_n$ polymers. It is noteworthy that the L/R_c values are larger than 0.72 indicating that the star-like micellar model is the most appropriate to describe the structure of the aggregates.[53] The formation of micelles of smaller cores (higher curvature) and larger corona thickness can be attributed to the bulkier polyglycidol chains, which tend to take larger space in the corona region compared to that of PEG of comparable degrees of polymerization. The areas, which the polyglycidol chains occupy on the core/corona interface, S_1, and on the outermost interface of the micelles, S_2, were calculated using the values of R_c and the experimental data for R_h and N_{agg} (Scheme 3). They are collected in Table 5 together with the values for micelles of related polymers based on PEG.

Polymer chains tethered to a highly curved core are less stretched than similar structures in a planar surface with equivalent tethering density as a consequence of the increase in the volume accessible to the tethered chains along the distance from the core.[54] Such chains can be considered as composed of several blobs with size that is an increasing function of corona thickness. Structures like this can be approximated to a truncated cone (Scheme 3), the volume of which can be calculated knowing the interface areas S_1 and S_2 as well as the corona thickness L. Data are given in Table 5. It is immediately seen from Table 5 that for the polymers, which have the same lipid-mimetic anchor (lines 1–8, Table 5) and at equal DPs of the polymer chains, both S_1 and S_2 are larger for the polyglycidol chains (compare line 2 with line 5 and line 3 with line 7 of Table 5). The difference is not so big for the couple DDP-$(G)_{110}$/DDP-$(EO)_{92}$, which are still of comparable DPs (lines 4 and 8 of Table 5), most probably due to the different stretching of the chains. The situation is a bit different when the PEG–lipids are considered (lines 9–11, Table 5). Here, the anchor is considerably larger: it is based on distearoyl phosphatidylethanolamine

Table 4 Values of core volume (V_c), core radius (R_c), corona thickness (L), corona thickness-to-core radius ratio (L/R_c) of spherical micelles formed by DDP-$(G)_n$ polymers (n = 23–110) and related polymers based on PEG

No	Polymer	V_c (Å^3)	R_c (Å)	L (Å)	L/R_c
1	DDP-$(G)_{23}$	72927	25.9	26.1	1.01
2	DDP-$(G)_{30}$	33659	20.0	31.0	1.55
3	DDP-$(G)_{54}$	24843	18.1	46.9	2.59
4	DDP-$(G)_{110}$	17631	16.1	62.9	3.91
5[a]	DDP-$(EO)_{30}$	58502	24.1	28.0	1.16
6[a]	DDP-$(EO)_{44}$	63311	24.7	38.0	1.54
7[a]	DDP-$(EO)_{52}$	44077	21.9	44.6	2.04
8[a]	DDP-$(EO)_{92}$	19234	16.6	48.4	2.92
9[b]	PEG750–DSPE[c] (DP = 17)	—	—	17.0	0.51
10[b]	PEG2000–DSPE[c] (DP = 45)	—	—	35.0	1.09
11[b]	PEG5000–DSPE[c] (DP = 114)	—	—	75.0	2.32

[a] Calculated using data taken from ref. 23 and 13. [b] Calculated using data taken from ref. 23 and 13. [c] Distearoyl phosphatidylethanolamine (DSPE).

Table 5 Values of areas occupied by polymer chains on the core/corona interface (S_1) and on the outermost interface of the micelles (S_2) of spherical micelles formed by DDP-$(G)_n$ polymers (n = 23–110) and related polymers based on PEG. V_{chain} is the space that the polymer chains occupy in the corona region

No	Polymer	S_1 (Å^2)	S_2 (Å^2)	V_{chain} (Å^3)
1	DDP-$(G)_{23}$	92.6	373.4	5653
2	DDP-$(G)_{30}$	119.7	778.2	12410
3	DDP-$(G)_{54}$	132.8	1712.7	36176
4	DDP-$(G)_{110}$	148.1	3565.0	93259
5[a]	DDP-$(EO)_{30}$	100.0	467.3	7287
6[a]	DDP-$(EO)_{44}$	97.0	625.3	12301
7[a]	DDP-$(EO)_{52}$	109.6	1010.4	21523
8[a]	DDP-$(EO)_{92}$	144.3	2212.2	47070
9[b]	PEG750–DSPE[c] (DP = 17)	159.6	359.2	4288
10[b]	PEG2000–DSPE[c] (DP = 45)	169.3	742.2	14766
11[b]	PEG5000–DSPE[c] (DP = 114)	167.1	1868.5	64934

[a] Calculated using data taken from ref. 23 and 13. [b] Calculated using data taken from ref. 23 and 13. [c] Distearoyl phosphatidylethanolamine (DSPE).

(DSPE), which is conjugated to PEG *via* carbamate linkage.[13] Accordingly, the S_1 values (in the 159–169 Å^2 range) are invariably larger than those of the polymers with the DDP anchor (Table 5). The S_2 values for the PEG–lipids are also generally larger if the PEG-based polymers only are considered (an exception is the couple PEG5000–lipid/DDP-$(EO)_{92}$, lines 8 and 11 of Table 5), however, invariably lower compared to the S_2 values for the polyglycidol-based polymers. Obviously, S_1 and S_2 reflect the influence of both the size of the lipid-mimetic anchor and the bulkiness of the polymer chain. The influence of these two factors is also seen in the space that the polymer chains occupy in the corona, V_{chain} (Table 5). For the polymers with the DDP anchor, the PEO chains occupy 41.3–49.5% smaller space than the corresponding polyglycidol chains (lines 2 and 5, 3 and 7, 4 and 8, Table 5). This is compatible with the smaller volume of the EO unit: 36.3% smaller volume calculated from the volumes of the component groups of the EO and glycidol units. The larger DSPE anchor takes larger area at the core–corona interface thus creating more space for the PEG chain. Accordingly, the latter occupies space that is only 30.3% smaller than that of the corresponding polyglycidol chain (lines 4 and 11, Table 5).

Self-assembly of DDP-$(G)_8$ and nature of its aggregates

DDP-$(G)_8$, the polymer of the lowest DP of the polymer chain, is unique amongst the rest of the polymers studied because it forms considerably larger particles. The relaxation time distribution (Fig. 7a) is considerably broader than those of the rest of DDP-$(G)_n$ polymers and seemingly composed of two modes. The software is not able to discriminate between the two modes, most probably because the particles, responsible for them are very close in hydrodynamic dimensions. The mean particle size was determined following the routine procedure for determination of the diffusion coefficients (see ESI†). The hydrodynamic radius of the particles that DDP-$(G)_8$ forms was calculated using the equation of Stokes–Einstein assuming a spherical shape. Data for D_0 and R_h are collected in Table 6. As the particles were large, a strong angular dependence of the quantity Kc/R_θ was observed. However, Kc/R_θ was not linearly dependent on $\sin^2(\theta/2)$ and, accordingly, the static light scattering parameters could not be defined by the Zimm plot method. Therefore, they were evaluated by the Berry plot method, which is applicable for strongly interacting species.[55] The Berry plot for DDP-$(G)_8$ in aqueous solution is shown in Fig. 7b and the derived parameters are listed in Table 6. Although still positive, indicating that the interparticle interactions are repulsive, the second virial coefficient is an order of magnitude lower compared to those of the micellar aggregates in Table 3. The small value of A_2 (practically close to zero) is in line with the high particle molar mass. The latter corresponds to a huge aggregation number – hundreds of thousands macromolecules per particle (Table 6), which fits perfectly to the exponential increase of N_{agg} with decreasing DP of polyglycidol chain (Fig. 6). The large R_g is noteworthy as well. It produces a value of R_g/R_h above 2 (Table 6), which implies formation of anisotropic, elongated particles. The high value can be attributed also to overestimation of R_g and hence R_g/R_h due to the seemingly broad size distribution (Fig. 7a).

An obvious question that arises from the results is what is the nature of the particles that DDP-$(G)_8$ forms. They can not be core–corona micelles as those that the rest of DDP-$(G)_n$ polymers as well as PEG–lipids form because of their huge dimensions. Moreover, if A_2 and M_w are used to express the equivalent hard sphere radius, R_{HS}, according to eqn (5),[56] a fairly inconsistent value of 267 nm is obtained in contrast to the reasonable agreement between R_{HS} and R_h observed for the core–corona micelles of the polymers DDP-$(G)_{23}$, DDP-$(G)_{30}$, DDP-$(G)_{54}$ and DDP-$(G)_{110}$. Furthermore, the huge aggregation number may indicate formation of worm-like micelles, which is partially supported by the high R_g/R_h value, or non-micellar structures such as bilayer disks and/or vesicles.

$$R_{HS} = \left(\frac{3A_2M_W{}^2}{16\pi N_A}\right)^{\frac{1}{3}} \quad (5)$$

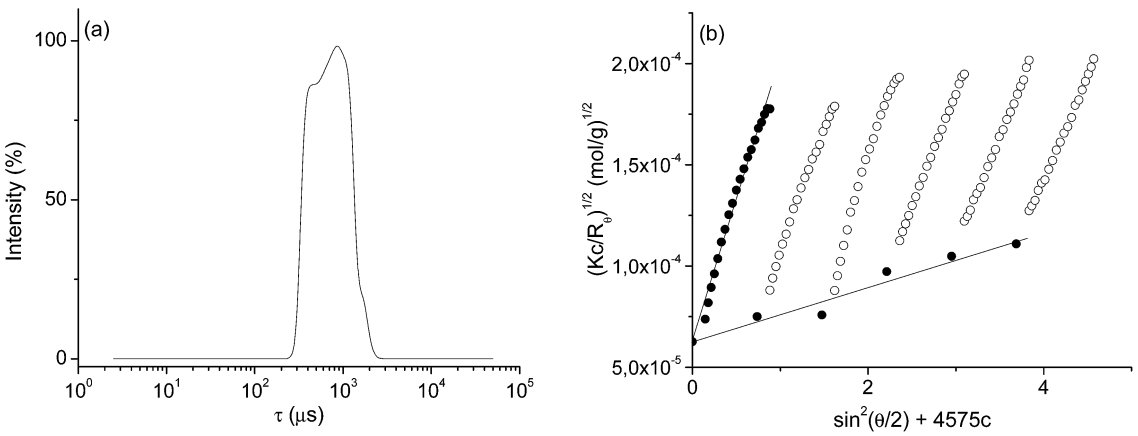

Fig. 7 (a) Representative relaxation time distribution measured at an angle of 90° for aqueous solution of DDP-$(G)_8$ at $c = 0.806$ mg mL^{-1} and 25 °C. (b) Berry plot of DDP-$(G)_8$ in water at 25 °C: experimental points (open symbols); extrapolated points (closed symbols).

Table 6 Characterization data and static and dynamic light scattering parameters of nonionic DDP-$(G)_8$ aggregates in water at 25 °C

$10^{11}D_0$ (m^2 s^{-1})	R_h (nm)	10^5A_2 (mol mL g^{-2})	$10^{-8}M_w$ (g mol^{-1})	$10^{-3}N_{agg}$ [a]	R_g (nm)	R_g/R_h
0.365	67.2	0.521	1.92	175	138.5	2.06

[a] Aggregation number.

It has repeatedly been observed by different research groups that the PEG-derivatized lipids in aqueous solution form lamellar phases together with small spherical micelles.[1,9,10,13,23,49–51] The former are typically observable in dynamic light scattering measurements as a slowly relaxing diffusive component of relatively low intensity with hydrodynamic radii exceeding tens even hundreds of nanometers. Logically, based on simple geometric considerations, the PEG-derivatized lipids with low DPs of PEG are more prone to form lamellar phases: it has been unambiguously shown that a lamellar phase is formed in dilute aqueous solution of PEG350–DSPE (DP = 8).[9] In the light of the above, we might expect such behavior of DDP-$(G)_8$. In the following we provide clear evidence for formation of lamellar aggregates using TEM and cryo-TEM to visualize the aggregates. Fig. 8 shows conventional TEM micrographs which are dominated by spherical objects with dimensions that are consistent with those from DLS. The material is damaged (large and numerous perforations) because it is very sensitive to the electron beam. However, its sensitivity and particularly the resulting perforations in the membrane revealing the empty interior allowed us to identify the vesicular structure of the particles.

Various structures were found in the cryo-TEM micrographs (Fig. 9). To prevent the damage caused by the electron beam, minimum exposure dose (*i.e.* the MDS microscope imaging option) was applied. It is visible that even at these conditions the material is still sensitive to the electron beam. However, the perforations occurred after relatively longer exposure to electron beam, which made it possible to visualize non-damaged or less-affected objects. The objects, which are observable in Fig. 9, exhibit dispersity in size, shape, and morphology. Spherical particles of vesicular structure with clearly distinguishable rims at the outermost periphery (Fig. 9a) were found to co-exist with a fraction of flat anisotropic structures of irregular shape (Fig. 9b). Both the size dispersity and co-existing morphology probably contribute to different extents to the high R_g/R_h value derived from the light scattering experiments (see above). Perforations were occasionally observed (white arrows in Fig. 9b); however, their size and number gradually increased with increasing exposure time. It is noteworthy that micellar phase (small spherical micelles) was not observed in any of these samples. The larger flat objects as those denoted with arrows A in Fig. 9b are observable mostly face-on since they are preferentially oriented parallel to the surface of the thinnest part of the vitrified film. The smaller objects of similar structure are observable also edge-on (arrows B in Fig. 9b). A rough estimation of the thickness of the flat objects gave a value of about 60 Å which is compatible with the membrane thickness of the vesicles in Fig. 9a.

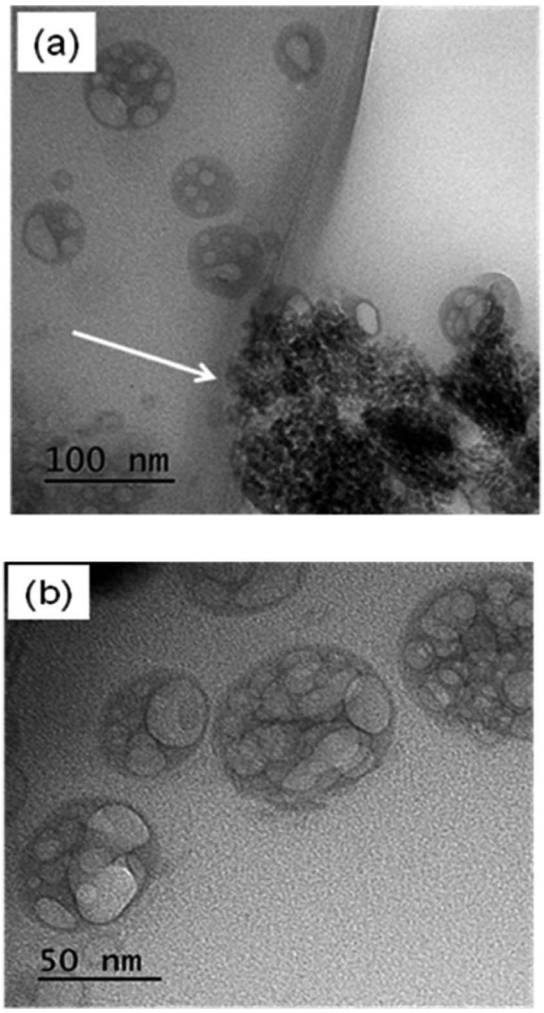

Fig. 8 Conventional TEM micrographs of samples taken from dispersion of DDP-$(G)_8$ in water, prepared at 25 °C and concentration of 5 mg mL^{-1}. Images (a) and (b) show different objects that are damaged by the electron beam. The dispersion was prepared at 25 °C and concentration of 5 mg mL^{-1}. The perforations revealing the vesicular structure are in strong contrast with the damages observed in the huge and dense (not hollow structure) object indicated with an arrow in (a).

The aqueous dispersions of DDP-$(G)_8$ were studied by SAXS. Fig. 10a shows a representative scattering curve taken at 25 °C. The data at $q > 0.015$ $Å^{-1}$ were analysed by the indirect Fourier transformation (IFT) method with the approximation of infinitely thin non-interactive objects.[57] More details for the

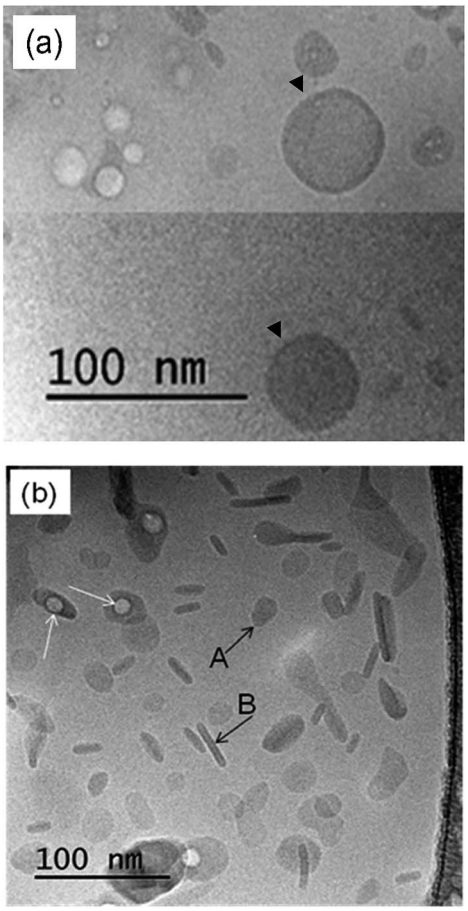

Fig. 9 Cryo-TEM micrographs of samples taken from dispersion of DDP-$(G)_8$ in water, prepared at 25 °C and concentration of 5 mg mL^{-1}. Images (a) and (b) show different types of structures that are size-segregated due to thickness variations in the specimen films. Large spherical particles of vesicular structure with a clearly distinguishable membrane denoted with arrowheads are observable in the thicker parts of the film (a), whereas the smaller and flat objects are located in the thinner parts (b). The dispersion was prepared at 25 °C and concentration of 5 mg mL^{-1}. Spherical particles of vesicular structure with a clearly distinguishable membrane are denoted with arrowhead on (a). Arrows A and B show objects observable face-on and edge-on, respectively. White arrows in (b) indicate damages (perforations) caused by the electron beam.

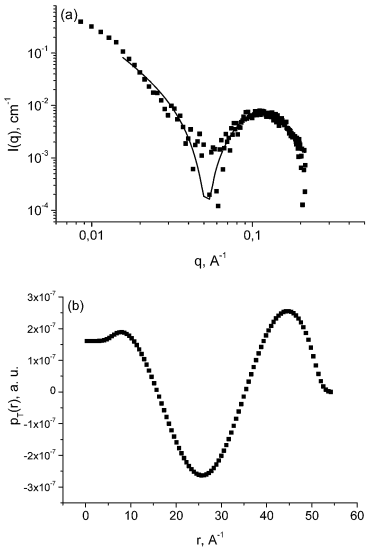

Fig. 10 (a) SAXS data for a 5 mg mL^{-1} dispersion of DDP-$(G)_8$ in water at 25 °C together with the fit of the IFT analysis (solid line). (b) Pair distance distribution function of thickness $p_T(r)$ obtained from the SAXS data.

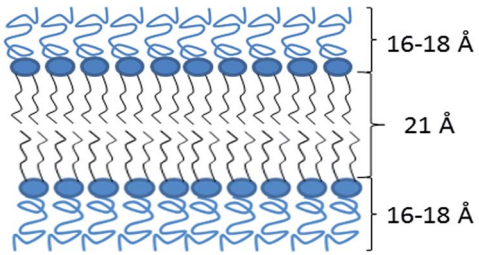

Scheme 4 Schematic presentation of a bilayer membrane formed by DDP-$(G)_8$ with the corresponding thicknesses of the hydrocarbon and polyglycidol sublayers.

analysis are given in ESI.† The best fit was obtained with layer thickness of 55 Å. The corresponding pair distance distribution function of thickness, $p_T(r)$, exhibited negative and positive values thus indicating that the scattering length density contrast varied within the different parts of the membrane (Fig. 10b). Assuming a sandwich-like structure of the membrane, composed of an inner hydrocarbon layer and two outer polyglycidol layers (Scheme 4), it was possible to estimate the thicknesses of the sublayers. The quantities that were obtained were 21 Å for the hydrocarbon chain layer and 16–18 Å for each of the two outer layers. The results are in full agreement with recent results for the hydrocarbon thickness of dilauroylphosphatidylcholine (the same number of carbons) lipid bilayers,[58] which ruled out possible formation of interdigitated bilayer membrane, as such a structure would be considerably thinner.

To get independent evidence for the presence of particles of vesicular structure in the DDP-$(G)_8$ dispersions, a leakage assay using a hydrophilic dye, 5(6)-carboxyfluorescein (CF), was carried out. The particles were prepared in an aqueous medium containing 100 mM of CF at which its fluorescence intensity is low due to self-quenching. The preparation protocol resulted in particles (presumably vesicles) containing CF at high concentration dispersed in a medium with no CF. The results from the leakage assay are presented in Fig. 11a as a plot of the fluorescence intensity *vs.* time. As the dye leaked out, it became diluted and the fluorescence intensity increased. The leakage was followed on the time scale of several hours, for which approximately 88% of the loaded CF was released. In a comparative experiment with an aqueous dispersion of the micelle-forming DDP-$(G)_{54}$, it was found that the polyglycidol corona displayed release-like behavior implying binding or partition of CF in the corona (Fig. 11b). However, after lysis with a surfactant, the fluorescence intensity sharply decreased in strong contrast to

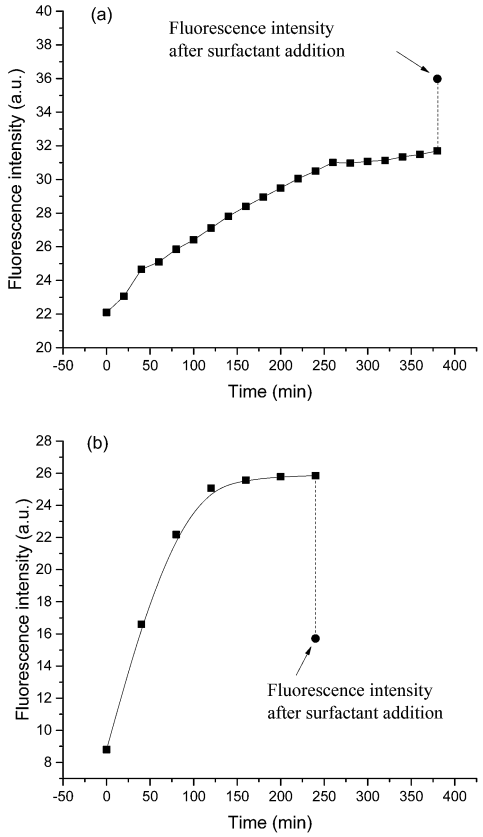

Fig. 11 Leakage of 5(6)-carboxyfluorescein from DDP-$(G)_8$ (a) and DDP-$(G)_{54}$ (b) particles. c = 5 mg mL^{-1}. Measurements were performed at 37 °C.

the experiment with DDP-$(G)_8$. The leakage assay unambiguously proved the existence of internal aqueous compartments in the particles of the latter polymer and, consequently, their vesicular structure. The entrapment efficiency of DDP-$(G)_8$ particles compared to that of other vesicles such as conventional liposomes was substantially lower. The reason, as shown above, is the formation of a fraction of non-vesicular bilayer structures (disks, flakes), which do not have reservoir function.

Conclusions

A series of five polyglycidol-derivatized lipids with degrees of polymerization of the linear polyglycidol moieties ranging from 8 to 110 were successfully prepared and their self-assembly in dilute aqueous solution was investigated. The thermodynamic data evidenced that the self-assembly in aqueous solution is an enthalpically disfavored endothermic process, for which the driving force was the positive entropy contribution. The CMC values were located in the lower millimolar region. They were slightly dependent on the temperature (decrease with increasing temperature) being most pronounced for the polymer of the highest degree of polymerization of the polyglycidol chain. This was attributed to partial coverage of the lipid-mimetic residue by the polyglycidol chain at lower temperatures and supposedly full exposure at elevated temperatures.

Polymers DDP-$(G)_{23}$, DDP-$(G)_{30}$, DDP-$(G)_{54}$, and DDP-$(G)_{110}$ formed small core–corona micelles, that were appropriately described by the star-like micellar model. Their hydrodynamic radii were found to increase with increasing degree of polymerization, whereas just the opposite was found for the aggregation number. The structural characteristics of the micelles were governed by the bulkiness of the polyglycidol chain. Accordingly, the micelles were characterized with smaller core radii and larger corona thickness compared to those of micelles of related polymers based on PEG. The larger areas that the polyglycidol chains occupied on the core/corona interface and on the outermost interface of the micelles as well as the volume in the corona region also reflected the effects of the bulky polyglycidol chain.

The polymer of the lowest DP of the polyglycidol chain – DDP-$(G)_8$ – formed co-existing lamellar structures, which were identified as closed spherical vesicles and elongated bilayer flakes. Their reservoir function of the former was evidenced by performing a leakage assay.

Acknowledgements

This work was supported by the National Science Fund (Bulgaria) Project Б 01/25 - 2012. The paper benefitted from the discussions at events of Precision Polymer Materials (P2M) Research Networking Programme of the European Science Foundation and from the European Commission project POLINNOVA.

References

1 G. Blume and G. Cevc, *Biochim. Biophys. Acta*, 1993, **1146**, 157.
2 M. C. Woodle and D. D. Lasic, *Biochim. Biophys. Acta*, 1992, **1113**, 171.
3 A. Klibanov, K. Maruyama, V. P. Torchilin and L. Huang, *FEBS Lett.*, 1990, **268**, 235.
4 M. Johnsson, N. Bergstrand and K. Edwards, *J. Liposome Res.*, 1999, **9**, 53.
5 D. D. Lasic, *Nature*, 1996, **380**, 561–562.
6 D. D. Lasic, J. J. Vallner and P. K. Working, *Curr. Opin. Mol. Ther.*, 1999, **1**, 177–185.
7 M. C. Woodle, *Adv. Drug Delivery Rev.*, 1995, **16**, 249–265.
8 V. P. Torchilin, *AAPS J.*, 2007, **9**, 128–147.
9 A. K. Kenworthy, S. A. Simon and T. J. McIntosh, *Biophys. J.*, 1995, **68**, 1903.
10 K. Edwards, M. Johnsson, G. Karlsson and M. Silvander, *Biophys. J.*, 1997, **73**, 258.
11 P. S. Uster, T. M. Allen, B. E. Daniel, C. J. Mendez, M. S. Newman and G. Z. Zhu, *FEBS Lett.*, 1996, **386**, 243.
12 K. Sou, T. Endo, S. Takeoka and E. Tsuchida, *Bioconjugate Chem.*, 2000, **11**, 372.
13 M. Johnsson, P. Hansson and K. Edwards, *J. Phys. Chem. B*, 2001, **105**, 8420–8430.
14 L. Vukovic, F. Khatib, S. P. Drake, A. Madriaga, K. S. Brandenburg, P. Kral and H. Onyuksel, *J. Am. Chem. Soc.*, 2011, **133**, 13481–13488.

15 S. M. Moghimi, I. Hamad, T. L. Andresen, K. Jorgensen and J. Szebeni, *FASEB J.*, 2006, **20**, 2591–2593.
16 M. Silvander, M. Johnsson and K. Edwards, *Chem. Phys. Lipids*, 1998, **97**, 15.
17 R. F. Flewelling and W. L. Hubbell, *Biophys. J.*, 1986, **49**, 531.
18 F. Bonte and R. L. Juliano, *Chem. Phys. Lipids*, 1986, **40**, 359–372.
19 A. Chonn, P. R. Cullis and D. V. Devine, *J. Immunol.*, 1991, **146**, 4234–4241.
20 R. K. Gupta, C. L. Varanelli, P. Griffin, D. F. Wallach and G. R. Siber, *Vaccine*, 1996, **14**, 219–225.
21 G. Bastiat, P. Oliger, G. Karlsson, K. Edwards and M. Lafleur, *Langmuir*, 2007, **23**, 7695–7699.
22 R. Mathur and P. Capasso, in Nonphospholipid Liposomes: Properties and Potential Use in Flavor Encapsulation, *Flavor Technology*, eds C.-T. Ho, C.-T. Tan and C.-H. Tong, American Chemical Society, Washington DC, 1997, ch. 17, pp. 219–230.
23 S. Rangelov, M. Almgren, Ch. Tsvetanov and K. Edwards, *Macromolecules*, 2002, **35**, 7074–7081.
24 O. K. Nag, V. R. Yadav, A. Hedrick and V. Awasthi, *Int. J. Pharm.*, 2013, **446**, 119–129.
25 T. R. Baekmark, T. Wiesenthal, P. Kuhn, T. M. Bayerl, O. Nuyken and R. Merkel, *Langmuir*, 1997, **13**, 5521.
26 T. R. Baekmark, T. Wiesenthal, P. Kuhn, A. Albersdorfer, O. Nuyken and R. Merkel, *Langmuir*, 1999, **15**, 3616.
27 T. Wiesenthal, T. R. Baekmark and R. Merkel, *Langmuir*, 1999, **15**, 6837.
28 H. Ahrens, T. R. Baekmark, R. Merkel, J. Schmitt, K. Graf, R. Raiteri and Ch. A. Helm, *ChemPhysChem*, 2000, **2**, 101–106.
29 D. N. T. Hay, P. G. Rickert, S. Seifert and M. A. Firestone, *J. Am. Chem. Soc.*, 2004, **126**, 2290–2291.
30 R. K. Kainthan, J. Janzen, E. Levin, D. V. Devine and D. E. Brooks, *Biomacromolecules*, 2006, **7**, 703–709.
31 S. Halacheva, S. Rangelov and Ch. Tsvetanov, *Macromolecules*, 2006, **39**, 6845–6852.
32 S. Rangelov, M. Almgren, S. Halacheva and Ch. Tsvetanov, *J. Phys. Chem. C*, 2007, **111**, 13185–13191.
33 S. Halacheva, S. Rangelov and V. Garamus, *Macromolecules*, 2007, **40**, 8015–8021.
34 S. Halacheva, S. Rangelov and Ch. Tsvetanov, *J. Phys. Chem. B*, 2008, **112**, 1899–1905.
35 S. Halacheva, S. Rangelov and Ch. Tsvetanov, *Macromolecules*, 2008, **41**, 7699–7705.
36 S. Rangelov, S. Halacheva, V. Garamus and M. Almgren, *Macromolecules*, 2008, **41**(22), 8885–8894.
37 S. Halacheva, S. Rangelov, Ch. Tsvetanov and V. M. Garamus, *Macromolecules*, 2010, **43**, 772–781.
38 S. Rangelov, E. Petrova, I. Berlinova and Ch. Tsvetanov, *Polymer*, 2001, **42**, 4483–4491.
39 A. Fitton, J. Hill, D. Jane and R. Miller, *Synthesis*, 1987, 1140–1142.
40 S. W. Provencher, *Macromol. Chem.*, 1979, **180**, 201–209.
41 P. Alexandridis, J. F. Holzwarth and T. A. Hatton, *Macromolecules*, 1994, **27**, 2414–2425.
42 A. Chattopadhyay and E. London, *Anal. Biochem.*, 1984, **139**, 408–412.
43 M. Svensson, P. Linse and F. Tjarneld, *Macromolecules*, 1995, **28**, 3597–3603.
44 M. Scherlund, A. Brodin and M. Malmsten, *Int. J. Pharm.*, 2000, **211**, 37–49.
45 S. Rangelov, E. Petrova, I. Berlinova and Ch. Tsvetanov, *Polymer*, 2001, **42**, 4483–4491.
46 S. Rangelov, B. Trzebicka, M. Jamroz-Piegza and A. Dworak, *J. Phys. Chem. B*, 2007, **111**, 11127–11133.
47 R. J. Hunter, *Foundations of Colloid Science*, Oxford University Press, New York, 1987, vol. 1.
48 N. Morone, T. Ueda, Y. Okumura, V. Rosilio, M. Haratake, N. Higashi, Z. Zheng and J. Sunamoto, *Polym. Prepr. (Am. Chem. Soc., Div. Polym. Chem.)*, 1998, **39**, 172.
49 D. D. Lasic, M. C. Woodle, F. J. Martin and T. Valentincic, *Period. Biol.*, 1991, **93**, 287.
50 R. Koynova, B. Tenchov and G. Rapp, *Colloids Surf., A*, 1999, **149**, 571.
51 V. S. Trubetskoy and V. P. Torchilin, *Adv. Drug Delivery Rev.*, 1995, **16**, 311.
52 J. F. Nagle and S. Tristram-Nagle, *Biochim. Biophys. Acta*, 2000, **1469**, 159.
53 J. P. S. Farinha, J. M. R. d'Oliveira, J. M. G. Martinho, R. Xu and M. A. Winnik, *Langmuir*, 1998, **14**, 2291.
54 M. Daoud and J. P. Cotton, *J. Phys.*, 1982, **43**, 531.
55 G. C. Berry, *J. Phys. Chem.*, 1966, **44**, 4550.
56 W. H. Richtering, W. Burchard, E. Jahns and H. Finkelmann, *J. Phys. Chem.*, 1988, **92**, 6032.
57 O. Glatter, *J. Appl. Crystallogr.*, 1977, **10**, 415.
58 N. Kucerka, Y. Liu, N. Chu, H. I. Petrache, S. Tristram-Nagle and J. F. Nagle, *Biophys. J.*, 2005, **88**, 2626.